Heliyon 10 (2024) e40706

Contents lists available at ScienceDirect

Heliyon

journal homepage: www.cell.com/heliyon

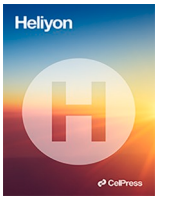

Research article

Property evaluation of graphene - reinforced Al-Cu-Li (2195) alloy for lightweight structural applications

M. Venkatraman , M. Anthony Xavior *

School of Mechanical Engineering, Vellore Institute of Technology, Vellore, 632014, Tamil Nadu, India

ARTICLE INFO

Keywords:
Graphene
Metal matrix composites
Mechanical properties
Microstructural analysis
Liquid composite moulding

ABSTRACT

Aluminium 2XXX series are prominently used in aerospace structural applications, especially Al-Cu-Li Alloys, which are used in the space exploration sector. This work aims to identify a substitute material and an effective manufacturing technique for producing suitable metal matrix composites intended for super lightweight tank structural applications. This work describes the property evaluation of 0.5 wt% of graphene-reinforced AA2195 composite processed through vacuum induction melting (VIM) technique under a dynamic inert atmosphere. Thus, the fabricated final cast plate was homogenized and hot rolled following the T8 heat treatment process. Incorporating 0.5 wt% of 2D – Graphene Sheets resulted in a 33 % enhancement in UTS and a 40 % increase in HRB relative to the AA2195 parent alloy. EBSD and Transmission Kikuchi Diffraction (TKD) analysis confirmed that the Graphene Sheets are homogeneously dispersed throughout the composite plate.

1. Introduction

In recent years, aluminium lithium alloy is found to be widely used in space shuttle for super lightweight tank (SLWT) applications and aircraft manufacturing industries, due to significant fuel savings, increase in payloads, low density, high specific strength, and high specific stiffness [1,2]. With a focus on cryogenic tank applications in satellite launch vehicles, The AA2195 stands out as the optimal alloy because of its remarkable cryogenic characteristics. Alloys containing lithium are the main competitor of Al–Cu–Mn/Al–Cu–Mg and Al– Zn–Mg–Cu subsystems because of their excellent mechanical properties in ambient and cryogenic temperatures [3,4]. Furthermore, the AA 2195 is a heat-treatable alloy and, when the alloy undergoes heat treatment, it exhibits increased mechanical properties and unique microstructural characteristics [5]. The developed nanocomposites with a refined microstructure strengthened the bonding between particles and matrix. Graphene is a highly promising material that is considered as reinforcement while developing the Metal Matrix Composites (MMCs) used for space exploration sectors compared with other ceramic reinforcements such as carbides and oxides [6,7]. Graphene-based aluminium alloy composites can satisfy the needs of aerospace external fuel tank structural applications as they meet the higher strength-to-weight ratio criterion. Graphene-doped metal matrix composites exhibit superior mechanical properties compared to conventional alloys, which is attributed to their fine-grain microstructure, making them highly suitable for structural applications in launch vehicle fuel tanks [8]. It has been reported that 0.5 wt percent of graphene sheets are homogenously dispersed in Aluminium Metal Matrix Composites (Al–MMCs) and have achieved strong interfacial bonding. This is necessary to fulfill the property requirements of the fuel tank structural application, as well as to make full use of the excellent

* Corresponding author.
E-mail address: manthonyxavior@vit.ac.in (M.A. Xavior).

https://doi.org/10.1016/j.heliyon.2024.e40706
Received 29 February 2024; Received in revised form 22 November 2024; Accepted 25 November 2024
Available online 26 November 2024

properties offered by the reinforced graphene sheets [9,10]. Graphene is one of the excellent reinforcement materials for aluminium based metal matrix composites because it has a good specific surface area which enhances the load transfer mechanism between particle to particle. When compared to carbon nanotubes, graphene seems to be superior for the fabrication of 2XXX metal matrix composites [11]. The method of hot rolling is a secondary forming technique that involves moving blocks between the rolls in order to get the desired thickness and shape. Strips, sheets, and foils are all products that can be made with it. Hot rolling is a technique used for processing metal matrix composites into plates of required thickness in the presence of a heat source. And it happens nearly at the recrystallization temperature of the matrix material. During the process, the strain-hardening effect is reduced and it allows the metal to become more pliable. As a result, a significant amount of deformation can be obtained on the hot-rolled composites [12]. However, only limited studies are reported on the hot rolling process of graphene-reinforced Al–Cu–Li alloy composites fabricated through the casting process. This work investigates the physical and mechanical properties of hot rolled composite plates fabricated with 0.5 wt% of graphene reinforcement on Al-Cu-Li (2195) alloy. Furthermore, this study aims to establish a new generation of lightweight composite materials that are not only sustainable but also exceptionally robust, redefining the standards for large-scale hydrogen storage in Super Lightweight Fuel Tank (SLWT) structural applications and the space exploration sector.

2. Materials and methods

2.1. Preparation of graphene-reinforced AA2195 composite material

The composite was fabricated using Aluminum alloy 2915 material the ingot was procured from Constellium Manufacturing Inc., USA. The chemical composition of AA2195 is provided in Table 1. Two-dimensional (2D) graphene sheets were procured from Angstron Materials Inc., USA, with a specific surface area of approximately 600 m^2/g of 2–3 layers, dimensions of 10 μm in length and 5 nm in thickness which is shown in Fig. 1. The molten metal was prepared using the vacuum induction melting furnace (VIM), with a dynamic argon (Ar) gas atmosphere. This method can prevent the gas porosity of molten metal with the help of a vacuum atmosphere and it ensures the uniform melting of AA2195 ingot [5]. Before placing the AA2195 ingot into the furnace chamber, the inner walls of the melting chamber were coated with a nano-graphite paste to prevent unwanted reactions between the furnace walls and the molten metal [13]. During the melting process, the furnace temperature was 750 °C for the complete melting of the AA2195 ingot. Once the complete melting of aluminium ingot is ensured the graphene sheets are gradually added into the liquid mould. The pitched-type turbine blade mechanical stirrer was used to stir the graphene-reinforced aluminum molten metal at 500 rpm for 5 min to ensure the homogeneous mixing of graphene sheets. This type of blade helps to generate a whirlpool vortex that draws the reinforcements are homogeneous mixing with liquid metals. A split mould designed and constructed in accordance with the ASTM B686/B686M standard using D2 die steel material was used for fabricating the composite samples [14]. The D2 die steel spilt mould was pre-heated to 400 °C to prevent the fast cooling of aluminium composite melt. The steel mould measures 200 mm in overall height, 100 mm in width, and has a thickness of 6.5 mm. After the composite melt was injected into the die, a compaction pressure of 110 MPa was utilized to produce the samples. Subsequently, the samples were cut into the required sizes using a wire electric discharge machine. The presence of lithium and graphene in the composite samples was ensured through optical emission spectroscopic (OES) analysis [15]. Fig. 2 presents the T8 heat treatment processes involved in this research work starting from the initial composite samples to the final stage including the hot rolling process.

2.2. Hot rolling process

The casted plate of 2D-graphene-reinforced AA2195 composites is sectioned into 50 × 50 × 6 mm3 square samples through wire electrical discharge machining (wire EDM) for the hot rolling operation. Before the rolling process, the samples undergo homogenization by being maintained at a temperature of 460 °C for a duration of 12 h for better nucleation growth between the matrix and alloying elements [16]. The Nabertherm L24/11 muffle furnace was used to heat the samples for the hot rolling operation, where an argon gas was applied within the furnace chamber to prevent surface metallurgical changes in the samples. The sample temperature was consistently maintained at 480 °C throughout each pass, with a heat ramp rate of 5 °C per minute. The rolling process is conducted using the New Field Laboratory Rolling Machine. The top and bottom rollers have a diameter of 105 mm, a rolling force of 1 N/mm, and operate at a speed of 10 revolutions per minute. The composite plate utilized in the hot rolling process possesses an initial thickness of 6 mm. The plate thickness reduction per pass is 0.1 mm, resulting in a final rolled composite plate thickness of 5.5 mm, as presented in Table 2. The calculated percentages of elongation in the rolling direction and transverse direction are 10 % and 8 %, respectively. The thickness reduction percentage is calculated to be 9 % [17].

Table 1
Chemical composition of AA2195.

Elements	Cu	Li	Ag	Mg	Zr	Fe	Si	Ti	Remaining
Wt%	3.8	1.1	0.6	0.5	0.15	0.12	0.1	0.1	Al

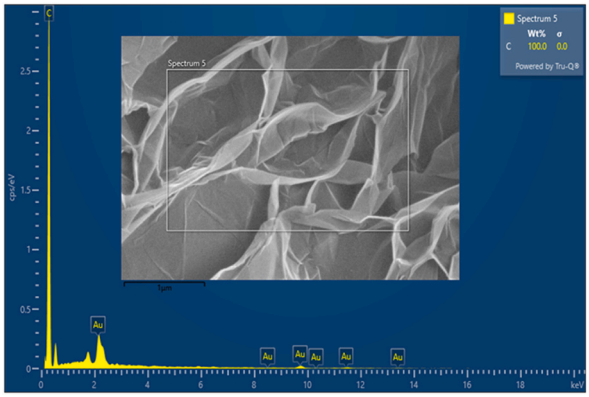

Fig. 1. Energy Dispersive Spectroscopy (EDS) analysis of 2D – Graphene sheet in received condition.

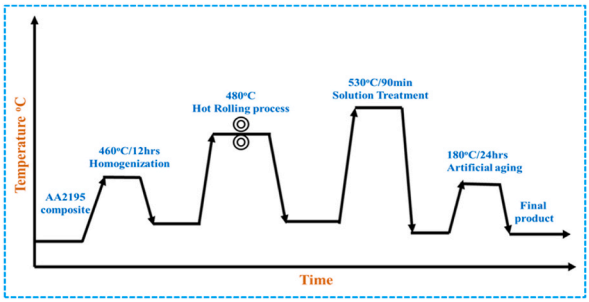

Fig. 2. T8 Heat Treatment Process adopted for AA2195 – Graphene composite.

Table 2
Rolling pass entrance and exit.

Pass	1st	2nd	3rd	4th	5th
Entrance (mm)	6	5.9	5.8	5.7	5.6
Exit (mm)	5.9	5.8	5.7	5.6	5.5

3. Results

3.1. Rockwell Hardness analysis

Table 3 represents the average Rockwell hardness values that were measured on 2D - graphene-reinforced AA2195 composite plates with various thicknesses (6.0–5.5 mm). An indenter made of a steel ball with a diameter of 1/16 mm, subjected to an imposed load of 100 kg-force for a duration of 10 s was used to measure the values in accordance with the ASTM E 18 for Rockwell Hardness B scale on metallic materials. The addition of 2D - graphene sheets followed by the heat treatment process resulted in an increase in the hardness of the composite plate. The hardness of the composite plate was a maximum of 83 HRB in the as-cast condition and a maximum of 119 HRB observed in hot-rolled by T8 condition, which is a 43 % increase due to the effective grain refinement and precipitation hardening for the T8 heat treatment process. Compared to the unreinforced parent alloy, the graphene-reinforced AA2195 composite is 40 % harder after hot rolling and T8 treatment. This enhanced hardness is attributed to the effective load transfer occurring between the matrix and reinforcement which is facilitated by the 2D - graphene sheets, Additionally, these graphene sheets act as barriers to dislocation movement [18,19].

Table 3
Rockwell hardness values.

Sample Description	Pure AA2195	AA2195 – Graphene composite in casted condition	AA2195 – Graphene composite in Hot Rolled by T8 condition
Rockwell Hardness (HRB)	85	83	119

3.2. Tensile properties

The tensile properties of a graphene-reinforced AA2195 composite plate rolled through five passes were observed for further analysis. The samples are prepared as per the ASTM E8/E8M standard and the test specimen size which is shown in Fig. 3(a). The ultimate tensile strength (UTS) values were noted for the unreinforced AA2195 samples and compared with graphene-reinforced AA2195 hot rolled and T8 aged samples. The composite samples were prepared by rolling direction (RD), inclined direction (ID), and transverse direction (TD) which are shown in Fig. 3(b), and the values are compared with the average of 3 samples in each direction. The addition of 0.5 wt percentage of 2D-graphene sheets exhibits the UTS value of 448 MPa in the transverse direction (TD), 447 MPa in the inclined direction (ID), and 450 MPa in the rolling direction (RD) which is shown in Fig. 4. It is well understood that the composite plate contains isotropic properties and the graphene sheets have enhanced the mechanical properties [20]. The UTS values decreased from 337 MPa to 240 MPa for graphene-reinforced as casted condition which is a decrease of 28 % compared with parent AA2195 in the T8 condition. During the solidification process casting results in a coarse grain structure and the formation of undesirable phases, such as intermetallic and eutectic constituents, which can impair the tensile properties. A coarse microstructure provides fewer barriers for dislocation movement so it reduces the composite tensile properties [21]. After the sample thickness reduction by 0.5 mm through the hot rolling operation (subjected to T8 heat treatment), the UTS value reached a maximum of 450 MPa. 33 % increment in the UTS values is exhibited by the hot rolled samples compared to unreinforced parent alloy. The yield point for the AA2195 composite can be determined using the proof stress method at a 0.02 % strain rate. The yield point, based on the data plot and using the origin, is 175 MPa for the as-cast condition. In the hot-rolled T8 condition, the yield points are 372 MPa in the rolling direction, 365 MPa in the inclined direction, and 368 MPa in the transverse direction. The percentage of elongation is 7.2 % in the as-cast condition, while in the hot-rolled T8 condition, it is 8.2 % in the rolling direction, 8.4 % in the inclined direction, and 8.2 % in the transverse direction which is shown in Table 4.

4. Discussion

4.1. XRD analysis

X-ray diffraction (XRD) analysis was carried out to determine the phase identification of the graphene-reinforced AA2195 composite plate which was analyzed on the hot rolled, solution treated in artificially aged by (T8) condition. As for the phase identification, the information was collected and compared with the JCPDS file, specifically for Al_4C_3 (35–0799), Al_2Cu (01-076-3073), Al_2CuLi (00-028-0011), and 2D - Graphene (00-008-0415) [22]. The XRD peaks validated the true presence of α-Al as a key matrix element in the final condition of the composite, as well as the peaks that demonstrate the presence of AA2195 and graphene mixture of the composite plate which is shown in Fig. 5. The graphene presence was observed at the angle of $2\theta = 42.4^{o}$, it is a successful incorporation of 2D - graphene sheets into the composite plate. The presence of these peaks suggests that the graphene sheets are integrated and interwoven within the composite structure. Furthermore, the final hot-rolled composite plate did not indicate any traces of aluminium carbide (Al_4C_3) formation. The absence of Al_4C_3 indicates that the fabrication process has effectively prevented undesirable reactions between the aluminum matrix and graphene sheets [23]. It also proves the successful fabrication of graphene-reinforced AA2195 composite plate in hot-rolled condition. The presence of α-Al and graphene phases along with the absence of aluminum carbide, validates the integrity and quality of the composite material. The XRD pattern uncovers the existence of equilibrium phases of θ-Al_2Cu and T1-Al_2CuLi intermetallic precipitates. This is crucial for enhancing the properties of aluminium alloys, particularly in those containing aluminum, copper, and lithium [24]. In the formation of these intermetallic compounds initially, two aluminum atoms are dissolved to create a supersaturated solid solution, subsequently, lithium and copper atoms precipitate out of the solution to form the θ-Al_2Cu and T1-Al_2CuLi phases [25]. These intermetallic phases are primarily observed near the grain boundaries due to the higher diffusion rates in these regions which can considerably change in the microstructure of the composite [26]. Furthermore, the T1 phase peaks are more pronounced in the composite compared to the unreinforced parent alloy indicating that the addition of graphene promotes the precipitation of this strengthening phase. The intensity of the T1 phase peaks is further enhanced by the combination of solution treatment followed by a subsequent aging process [27]. Finally, the alloy formation indicates that the angle of $2\theta = 42.5^{o}$ intermetallic precipitate of T1-Al_2CuLi suggests the formation of alloy phases, including the intermetallic and elemental peaks of aluminum, copper,

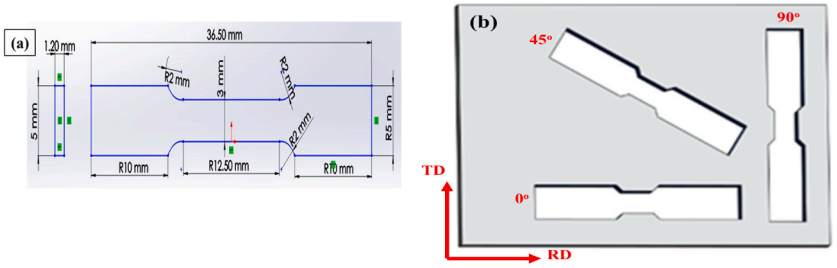

(a) Tensile specimen size (ASTM E8/E8M) **(b) sample preparation directions**

Fig. 3. (a) Tensile specimen size (ASTM E8/E8M) (b) sample preparation directions.

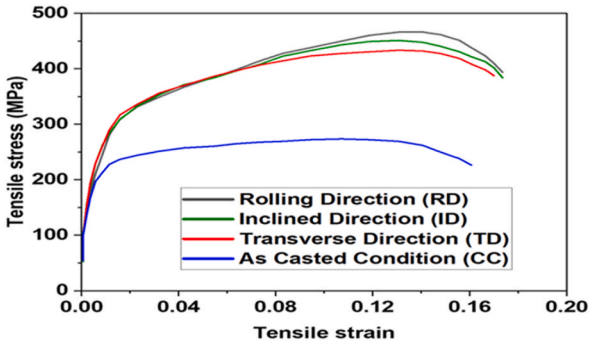

Fig. 4. Tensile stress Vs strain curve of the AA2195 – 0.5 wt% Graphene MMCs.

Table 4
Tensile properties of AA2195 – Graphene reinforced MMCs.

Sample description	Ultimate tensile strength (UTS) (MPa)	Yield strength (MPa)	% of Elongation	Scattering error (MPa)
AA2195 - Graphene composite (As - casted condition)	240	175	7.2	±5.00
Rolling Direction (RD)	450	372	8.2	±4.12
Inclined Direction (ID)	447	365	8.4	±3.60
Transverse Direction (TD)	448	368	8.2	±6.16

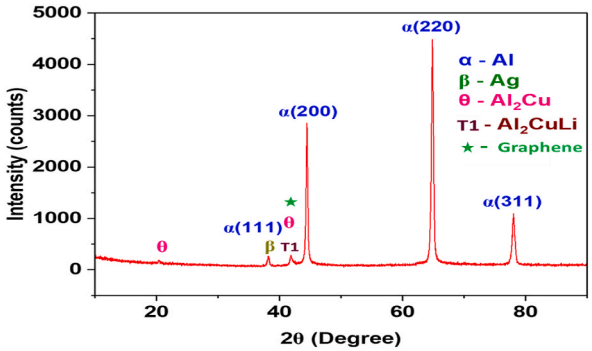

Fig. 5. XRD analysis of 2D - Graphene reinforced AA2195 composite hot rolled by (T8) condition.

lithium, and graphene. The peak shifts in these elements suggest alloy formation and interactions between aluminum and other alloying elements [28]. The results obtained are in line with those of the other researchers.

4.2. Microstructural analysis

The microstructure was obtained from a Hirox RH – 2000, digital microscope which provides both Two-dimensional (2D) and Three-dimensional (3D) imaging. The 0.5 wt% of graphene-reinforced Al-Cu-Li (AA 2195) composite was subjected to hot rolling and subsequent heat treatment process. This hot-rolled composite was examined for its microstructural characteristics and mechanical strength qualities. Fig. 6(a) shows the 2D microscopic image of the graphene-reinforced AA2195 composite plate in its as-cast condition, which indicates a dendritic microstructure. The average grain size was observed from the range of 120–125 μm, due to the normal solidification rate during the casting process. Fig. 6(b) shows the corresponding grain structure mapping of the as-casted condition which shows the individual grains of the composite along with the uniform dispersion of 2D - graphene sheets in the composite cast.

Fig. 6(c) Represents the microstructure of a hot rolled composite plate with 5.5 mm thickness (reduced from 6 mm to 5.5 mm). which shows the significant grain refrainment of the aluminium grains during the hot rolling process. This refinement is likely facilitated by graphene sheets, which could act as nucleation sites for new grains or promote the formation of more stable grain boundaries [29]. Fig. 6(d) shows the corresponding grain structure mapping of the hot rolled composite plate which clearly shows the elongation of both the aluminum grains and the graphene sheets along the rolling direction. This elongation is a result of the deformation provided by the hot-rolling process.

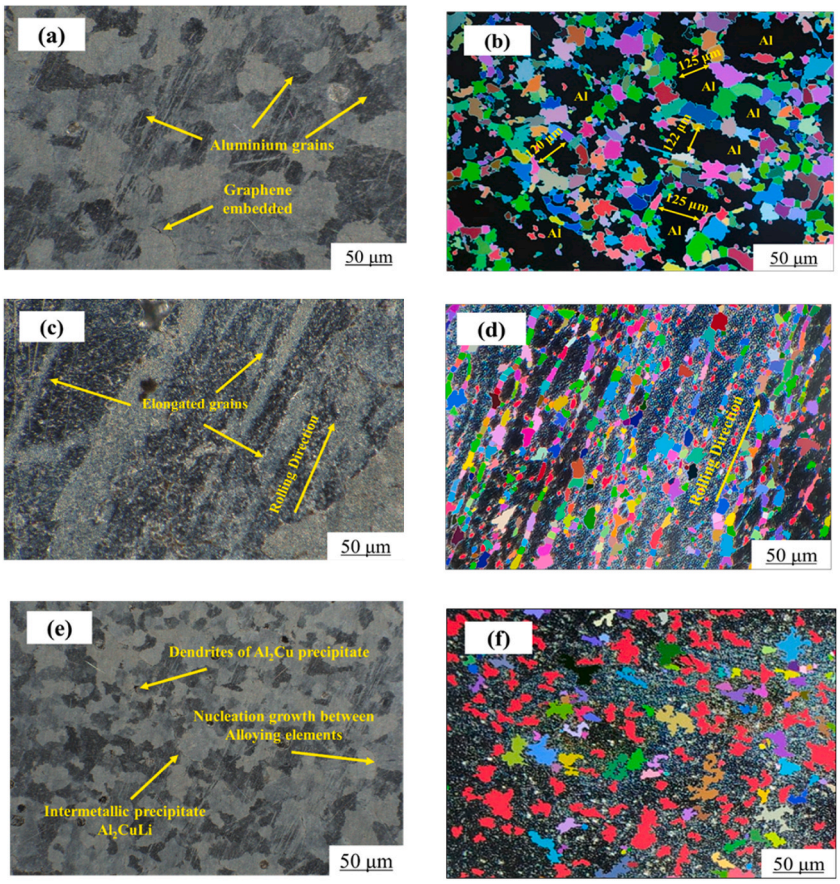

Fig. 6. Microstructure analysis of graphene reinforced AA2195 composite in (a) As-casted condition (b) corresponding grain structure mapping (c) Hot rolled condition (d) corresponding grain structure mapping (e) 180 °C for 24 h aged by T8 condition (f) corresponding grain structure mapping.

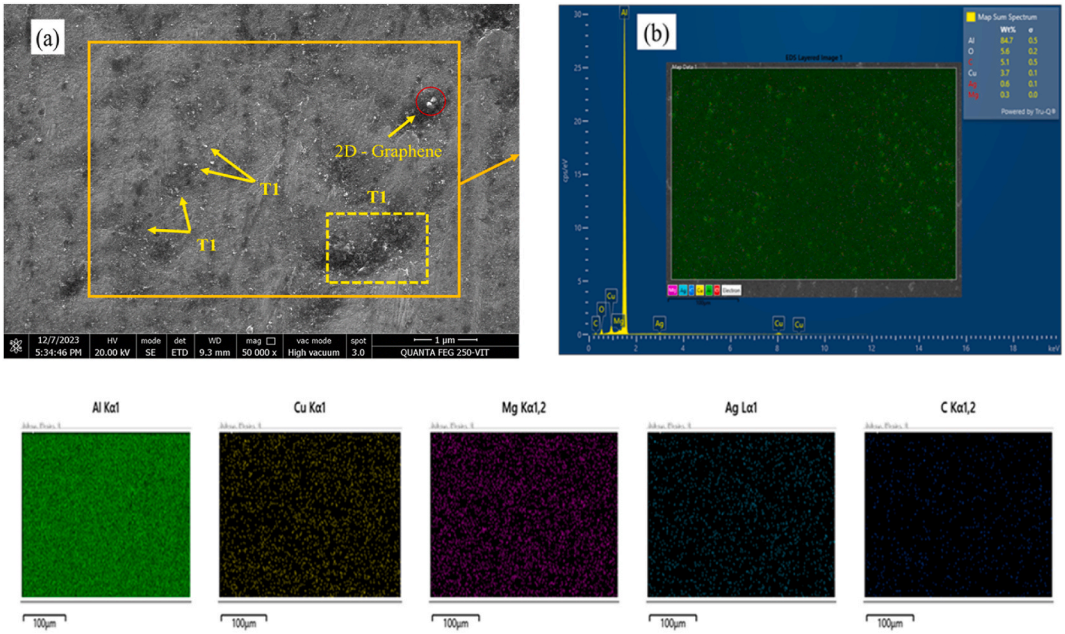

Fig. 7. (a) FE-SEM image of graphene reinforced AA2195 composite hot rolled by T8 condition (b) Energy Dispersive Spectroscopy (EDS) mapping.

Fig. 6(e) shows the microstructure of artificially aged (T8) condition of a 5.5 mm thick rolled plate on which the fine grain microstructure with an average grain size was observed 60–70 μm. Compared to the as-cast condition, the grain size of the composite was reduced by 44 % after the hot rolling and subsequent heat treatment process. The Al grains are observed to be encircled by the intermetallic secondary phases of the Al_2CuLi precipitate, while the graphene sheets have undergone significant alterations in grain morphology [30,31]. Fig. 6(f) shows the corresponding grain structure mapping of the artificially aged (T8) composite plate, which clearly shows the significant grain refinement compared to the as-cast condition. The map reveals the formation of stable precipitates of θ – Al_2Cu and T_1 – Al_2CuLi. Furthermore, this finding is supported by the Field Emission Scanning Electron Microscopy (FE-SEM) image in Fig. 7(a), This transformation is clearly understood by the addition of 0.5 wt% of graphene sheets and subsequent heat treatment process to facilitate the actual grain refinement which is being observed over the composite plate. Fig. 7(b) shows the Energy Dispersive Spectroscopy (EDS) analysis of uniform dispersion of graphene sheets within the composite in the hot rolled by T8 condition.

Fig. 8 shows the Transmission electron microscopy (TEM) investigation of AA2195 composite was hot rolled with T8 heat-treated condition which shows the atomic level microscopic image of the interaction between the graphene reinforcement and the aluminum matrix. Fig. 8(a) show the dark field (DF) image of θ′ precipitates of Al_2Cu and the presence of T1 needle-shaped precipitates of Al_2CuLi within the alloy matrix contributes significantly to the enhancement of material strength [32]. Fig. 8(b) represents the selected area electron diffraction (SAED) pattern of the graphene-reinforced AA2195 composite, revealing T_1 streaks that indicate the presence of T_1 precipitates within the composite. Furthermore, the secondary precipitates of the (δ’ + β′) phase are observed in the composite along with reflections from the (111) Al and (200) Al zone axes [22]. During the heat treatment process the precipitation sequence of (Al-Cu-Li) alloy without pre-stretching is solid solution strengthening (SSS) → Guinier Preston (GP) zone + δ′/β’ → θ′ + T1. This sequence indicates that the 2195 alloy undergoes a series of precipitation reactions. The process begins with the formation of a solid solution during solution treatment. As the alloy is aged for 180 °C in 24 h the Guinier-Preston (GP) zones form which are clusters of atoms that serve as precursors to further precipitates. Over time these GP zones evolve into the more stable θ′ phase (Al_2Cu) and the T1 phase (Al_2CuLi) [33]. The development of precipitates in the 2195 alloy is shaped not only by the T8 heat treatment process but also by the specific combination of the alloying elements and the presence of homogeneously dispersed 2D - graphene sheets to enhance the precipitate formation [34]. This precipitation sequence suggests that the mechanisms of precipitation hardening are similar across different alloys with the specific phases and sequences varying depending on the composition and heat treatment conditions. Additionally, the uniformly dispersed graphene sheets serve as nucleation sites to enhance the formation and distribution of these precipitates [35]. Fig. 8(c) shows the bright field (BF) image of the aluminium graphene interface in the alloy matrix which shows the single layer of graphene sheet with a clean surface area and no major defects it ensures effective reinforcement of the matrix material. The single-atomic layer of graphene sheets can reduce the spacing between the metal layers and enhance the coherent interface between the matrix. This closer packing of metal layers plays an important role in improving the mechanical properties [36]. The addition of 2D - graphene sheets into the AA2195 matrix can interrupt the grain growth due to re-nucleation by graphene sheets and create a finer grain structure which is known as the pinning effect. The pinning effect of graphene in metal matrix composites can be

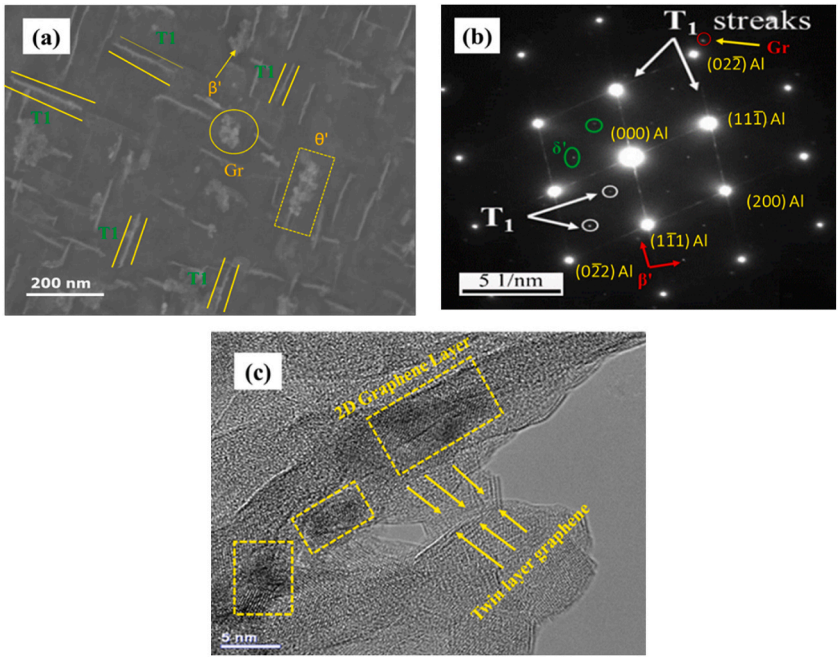

Fig. 8. (a) Dark field TEM image of 0.5 wt% of graphene reinforced AA2195 hot rolled composite plate at T8 condition (b) corresponding SAED pattern (c) Aluminium - Graphene interface in T8 condition.

enhanced by increasing the graphene content and decreasing its size. This is because graphene can effectively pin grain boundaries to prevent grains from growing leading to a finer grain structure [37]. Finally, the precipitation sequence for the T8-processed AA2195 graphene composite aligns well with the good agreement of other research studies.

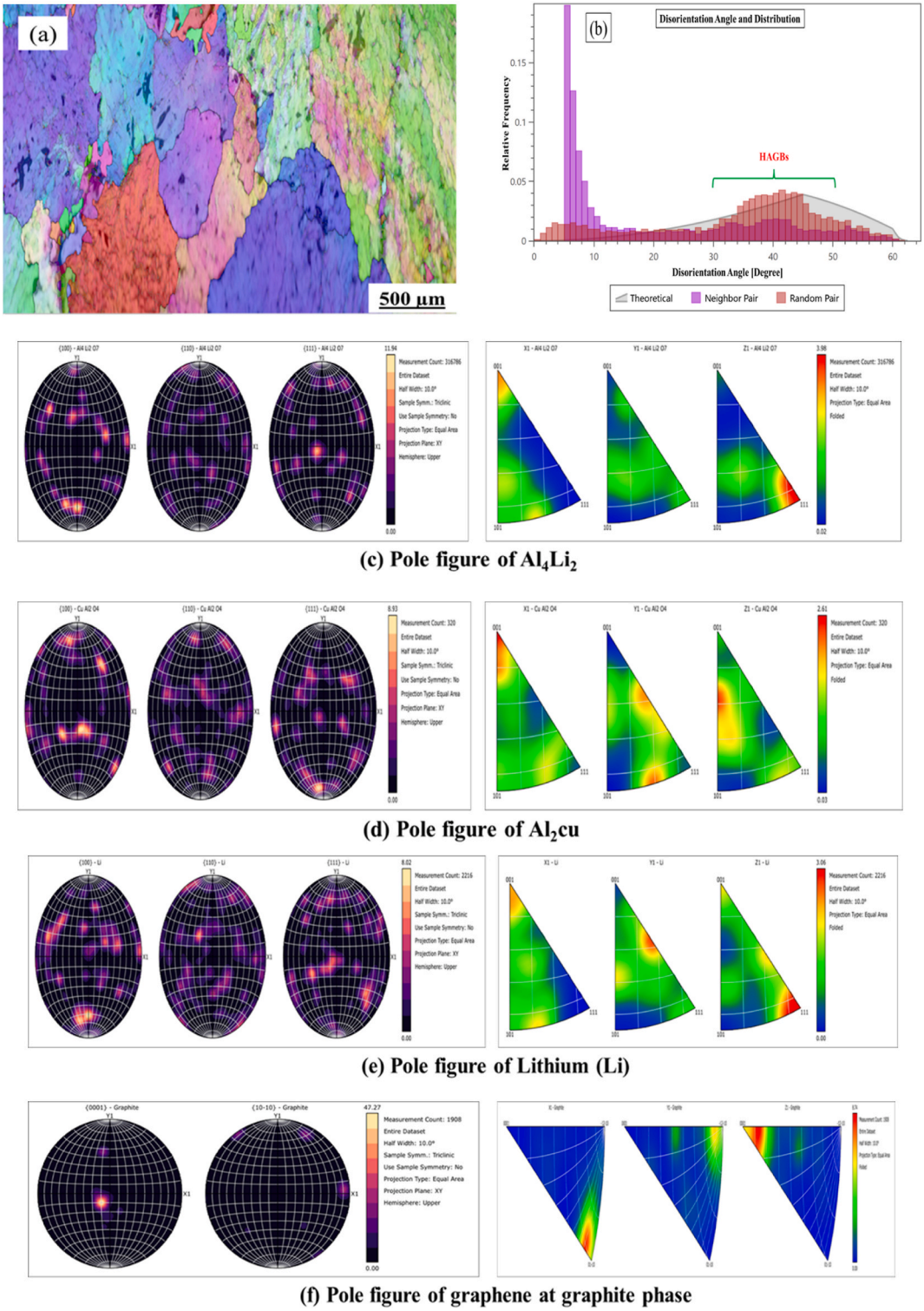

Fig. 9. The EBSD analysis of 0.5 wt% of graphene - AA2195 hot rolled plate at T8 condition (a) Grain boundaries map (b) Grain distribution (c) Pole figure of Al_4Li_2 (d) Pole figure of Al_2Cu (e) Pole figure of Lithium (f) Pole figure of graphene at graphite phase.

The Electron backscatter diffraction (EBSD) data shows information about the crystal structure orientation, grain elongation, average grain size, pole figures, disorientation angle, and grain borders of the produced plate. Fig. 9(a) presents the EBSD maps of individual grain boundaries of the hot rolled composite plate at T8 condition and it indicates the fine-grained microstructure structure. Additionally, the composite demonstrates a well-defined grain orientation, with a mixed structure of (101), (111), and (001) crystallographic planes. The incorporation of 0.5 wt % of 2D - graphene sheets to the AA2195 matrix has a significant effect on the microstructure of the composite, particularly in achieving ultra-fine grain boundaries and it also leads to the arrest of the dislocation movement of the MMCs. Furthermore, the graphene sheets are to promote better nucleation growth between the other alloying elements [38]. Fig. 9(b) shows the disorientation angle and distribution of grain boundaries, which indicates a high concentration of low-angle grain boundaries (LAGBs) in neighbor pairs within the range of (0°–30°). The Low-angle grain boundaries are formed during the plastic deformation of the composite in the hot rolling process. which is typical of grains that have been deformed but not fully recrystallized. The high-angle grain boundaries (HAGBs) are observed in random pairs between (30°–50°), which can act as a barrier to dislocation movements along with graphene sheets [39]. During the hot rolling process the significant improvement of closing the

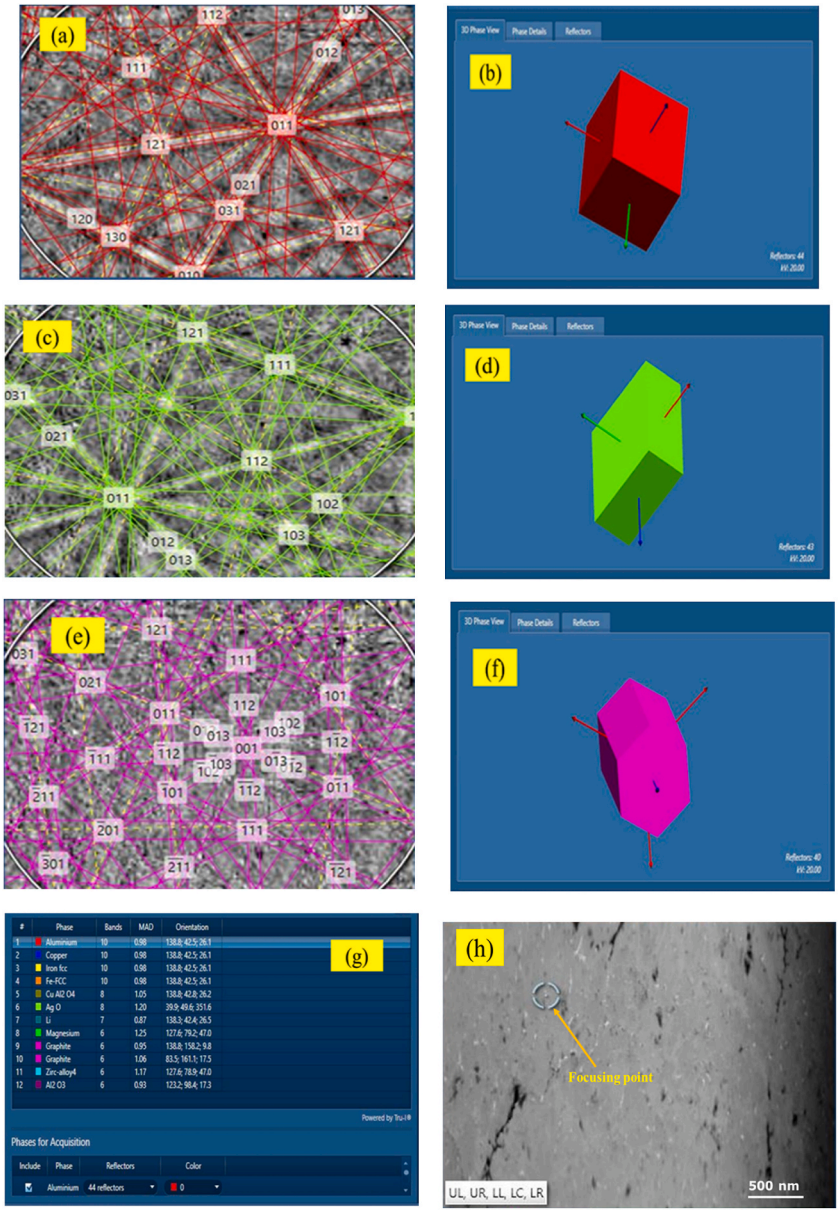

Fig. 10. (a) Kikuchi pattern of α-aluminium grain (b) lattice structure of α-aluminium grain (c) Kikuchi pattern of silver particles (d) lattice structure of silver particles (e) Kikuchi pattern of 2D - graphene sheets (f) lattice structure of 2D - graphene sheets (g) Mapping of lattice structures and plane orientation angles (h) TEM image of TKD analysis.

internal and surface micro-pores in the composite plate. This is likely due to the deformation and rearrangement of grains under the pressure and heat of the rolling process. By slightly elongating into needle shapes the grains can fill in voids and pores more effectively it also leads to a denser and more uniform microstructure of the composite plate [40]. During the aging process of 180 °C for 24 h various mechanism have been proposed by different research studies. The Possible mechanisms due to the graphene addition on AA2195 are the heterogeneous nucleation of 2D – graphene sheet based on equation (1). which are homogeneously dispersed and might act as nucleation sites for the T1 phases [37,38].

$$N_{het} = f_1 C_1 e^{\frac{\Delta G^*_{het}}{kT}} Nuclei \Big/ m^3 \quad (1)$$

Where;

N_{het} = r* = critical nucleus for heterogeneous nucleation of metal

f_1 = volume fraction of the particle at dispersed phase

ΔG^*_{het} = Total Gibbs free energy

C_1 = critical value for detectable nucleation

K = Rapid nucleation.

T = Specific temperature.

The formation of refined grains depends on the temperature and time profile of the composite plate [41]. The higher weight % of graphene sheets seems to be grouped together in the EBSD maps these grain boundaries may be weaker due to graphene agglomeration. However, EDS analysis of Fig. 7(b) confirms the uniform dispersion of graphene sheets within the composite plate. Furthermore, the EBSD analysis revealed the presence of intermetallic compounds Al_4Li_2 and θ - precipitates of Al_2Cu within the composite as shown in Fig. 9(c) and (d). Finally, the pole figures in Fig. 9(e) and (f) confirm the presence of lithium and graphene in the composite plate. It is evident that the graphene sheets act as an inhibitor pinning effect and restrict to the grain growth of the composite [42].

Transmission Kikuchi Diffraction (TKD) analysis is observed using a Charge-Coupled Device (CCD) detector through transmission electron microscopy (TEM) to analyze atomic arrangements within a crystal. Kikuchi lines represent the diffraction patterns formed by diffused electron scattering, with Bragg's law as the foundation for all diffraction phenomena, including Kikuchi patterns. These patterns reveal single-crystal diffraction and enable the identification of plane orientations, typically represented by Miller indices or reciprocal lattice notation which is given by equation (2) [43].

$$|K| = \frac{1}{d_{hkl}} = \frac{2\sin(\theta_B)}{\lambda} \quad (2)$$

Where;

$|K|$ - Represents the reciprocal lattice vector in crystallography, which is inversely related to the interplanar spacing d_{hkl}.

d_{hkl} - The interplanar spacing between planes in a crystal, denoted by the Miller indices *h*, *k*, *l* which specify the orientation of the planes in the crystal lattice.

λ - The wavelength of the X-rays used in the diffraction experiment.

θ_B - The Bragg angle, the angle at which X-rays are diffracted by the crystal planes.

$2\sin(\theta_B)$ - Relates to the geometry of constructive interference in the diffraction pattern.

The Kikuchi patterns are exhibit characteristic features are such as Kikuchi bands and their intersections, which are closely related to projections of crystallographic elements, namely the zone axes [*uvw*] and lattice planes (*hkl*) onto a planar screen [44]. The centers of the Kikuchi bands correspond to lattice planes, while intersections of these bands represent lattice directions. Variations in the geometric properties of Kikuchi patterns can be associated with changes in lattice parameter ratios, lattice rotations, and projection transformations [45].

Fig. 10(a) Explains the Transmission of Kikuchi Diffraction (TKD) for the 0.5 wt% of graphene-reinforced AA2195 hot-rolled composite plate that was artificially aged by T8 condition. The Kikuchi patterns reveal the primary matrix of α-aluminum grains within the composite. The well-defined Kikuchi lines indicate a highly crystalline structure in the composite plate, with clear intersection points showing planes associated with Miller indices of (111), (121), and (011), corresponding to a single crystal orientation along these zone axes [46]. Fig. 10(b) shows the lattice structure of the α-aluminum grains, which are observed to exhibit a face-centered cubic FCC structure. This is consistent with the inherent crystal structure of pure aluminum. It confirms the absence of aluminum oxide (Al_2O_3) and Al_4C_3 formations in the composite plate. The lack of these secondary phases suggests that the graphene reinforcement did not lead to undesirable reactions, thus preserving the integrity of the α-aluminum FCC lattice structure in the composite [47].

Fig. 10(c) shows the distribution of silver (Ag) as a secondary alloying element in the composite plate which is confirmed by the Kikuchi pattern analysis. The Kikuchi pattern distinct lines serve as evidence of silver's presence within the composite, which can help elucidate its role in the microstructure [48]. The formation of the lattice plane of (Ag) occurs along the (011), (121), and (111) axes, which is correspond with the specified Miller indices. This alignment suggest that silver (Ag) contributes significantly to composite structural refinement and stability [49,50]. Fig. 10(d) shows the lattice structure of the alloying element silver (Ag) within the composite, which is formed on the face-centered cubic (FCC) structure. Furthermore, there is an absence of Ag_2O formation in the final T8 heat-treated composite plate. This suggests that the heat treatment process was effective in maintaining the elemental state of silver without promoting oxidation [51].

Fig. 10(e) indicates the occurrence of the reinforcement material (2D - graphene sheets) in the AA2195 composite plate which is clearly evident from the Kikuchi pattern. These patterns formed were multiple axis points compared with other aluminium and silver patterns. It also proved that the 2D - graphene sheets are homogenously dispersed on the composite plate, which is also proved by the EDS mapping shown in Fig. 7(b). The intersection points of lines, such as (001), (101), and (112), correspond directly to atomic positions within the crystal lattice. Furthermore, these intersection points are aligned with the Miller indices (hkl) that define these crystallographic planes [52]. Fig. 10(f) shows the hexagonal close-packed (HCP) lattice structure of the graphene sheet, clearly showing its formation. The lattice arrangement and structure indicate that the graphene sheets are embedded and interlocked by their own nature. Finally, the TKD results closely resemble the XRD analysis, showing a strong correlation between the angle and intensity of the 2-theta values [53,54]. This mutual agreement between TKD and XRD confirms that the alloying elements have been fully recovered into the composite plate which is distinctly apparent from Fig. 10(g). Fig. 10(h) shows the marked focusing point indicating the specific area where Transmission Kikuchi Diffraction analysis (TKD) was conducted.

5. Conclusion

In this research work, 2D - graphene reinforced AA2195 composite plate was manufactured by vacuum induction melting process followed by hot rolling and heat treatment (T8 condition). The findings from the study are listed below.

1. The addition of 2D - graphene (reinforcement) and the lithium particles (available in the AA2195 alloy) are homogeneously dispersed in developed composite cast samples.
2. From the FESEM analysis and EDS mapping it has been inferred that the graphene sheets are distributed in a uniform manner throughout the AA2195 MMCs. In addition, the research demonstrated that the graphene sheets are incorporated and interlocked throughout the grain boundaries of the Al-Cu-Li (2195) matrix.
3. In the hot rolling operation, the refinement of aluminium grains in the rolled plate significantly enhances the mechanical properties of the produced composite. The incorporation of 0.5 wt% of 2D graphene sheets into AA2195 demonstrated an improvement in mechanical properties. such as an increase in hardness from 85 to 119 HRB and UTS from 337 MPa to 450 MPa at T8 condition.
4. The EBSD data further substantiates the spatial distribution of graphene and lithium particles within the AA2195-based composite. The incorporation of graphene sheets has markedly impeded crystallization throughout the post-deformation annealing process.
5. Transmission Kikuchi Diffraction (TKD) analysis also found that the Bragg's angle 42.5 deg for Al_2Cu and Li lies in the same angle evidently resembles the formation of alloy T1 – Al_2CuLi.
6. Compared to the unreinforced parent alloy the graphene-reinforced AA2195 composites dramatically increase the overall mechanical strength by the incorporation of just a tiny amount of graphene. However, the cost and scalability of producing graphene-reinforced alloys are slightly higher when compared to other composites.

Overall, the results of this research have contributed to a deeper understanding of the fabrication of MMC plates, characterized by a uniform distribution of graphene sheets and lithium particles, which are appropriate for large-scale production utilizing the vacuum induction melting technique. Consequently, this will function as an alternative fabrication technique for the production of lightweight metal matrix composites intended for super lightweight tank applications.

CRediT authorship contribution statement

M. Venkatraman: Writing – original draft, Methodology, Investigation, Formal analysis. **M. Anthony Xavior:** Writing – review & editing, Supervision, Methodology, Conceptualization.

Data availability statement

The data that support the findings of this study are available from the corresponding author upon reasonable request.

Ethics declarations

This research was conducted in strict compliance with all applicable rules, guidelines, and regulations.

Funding statement

This research was conducted without any specific funding support from public, commercial, or not-for-profit organizations.

Declaration of competing interest

The authors declare that they have no known competing financial interests or personal relationships that could have appeared to influence the work reported in this paper.

Acknowledgement

The authors would like to acknowledge Dr. Ashwath Pazhani, Lecturer in Engineering Design and Materials Specialism at Coventry University, UK, for his valuable technical assistance and guidance, which greatly contributed to the success of this project.

Appendix A. Supplementary data

Supplementary data to this article can be found online at https://doi.org/10.1016/j.heliyon.2024.e40706.

References

[1] S.Y. Duan, C.L. Wu, Z. Gao, L.M. Cha, T.W. Fan, J.H. Chen, Interfacial structure evolution of the growing composite precipitates in Al-Cu-Li alloys, Acta Mater. 129 (2017) 352e60.
[2] M. Xin, Z. Wang, B. Lu, Y. Li, Effects of different process parameters on microstructure evolution and mechanical properties of 2060 Al- Li alloy during vacuum centrifugal casting, J. Mater. Res. Technol. 21 (2022) 54e68.
[3] ASM specialty handbook, aluminum and aluminum alloys, in: J.R. Davis (Ed.), The Materials Information Society, Materials Park, ASM International, OH, 1998, pp. 121–142.
[4] J.R. Pickers, F.H. Heubaum, T.J. Langan, L.S. Kramer, in: T.H. Sanders Jr, E.A. Starke Jr (Eds.), Proceedings of the Fifth International Aluminum–Lithium Conference, Materials and Component Engineering Publications (MCEP), Williamsburg, Virginia, 1989, pp. 1397–1414.
[5] Niraj Nayan, S.V.S. Narayana Murty, Abhay K. Jha, Processing and characterization of Al–Cu–Li alloy AA2195 undergoing scale up production through the vacuum induction melting technique, Mater. Sci. Eng., A 576 (2013) 21–28.
[6] A.K. Srivastava, B. Sharma, B.R. Saju, A. Shukla, A. Saxena, N.K. Maurya, Effect of Graphene nanoparticles on microstructural and mechanical properties of aluminum-based nano composites fabricated by stir casting, World Journal of Engineering 17 (6) (2020) 859–866.
[7] T. Arunkumar, V. Pavanan, V.A. Murugesan, V. Mohanavel, K. Ramachandran, Influence of nanoparticles reinforcements on aluminium 6061 alloys fabricated via novel ultrasonic aided rheo-squeeze casting method, Met. Mater. Int. 28 (1) (2022) 145–154.
[8] C. Rao, U. Maitra, H. Matte, Synthesis, characterization, and selected properties of graphene, in: Graphene: Synthesis, Properties, and Phenomena, John Wiley & Sons, Hoboken, NJ, USA, 2013.
[9] A. Ramanathan, P.K. Krishnan, R. Muraliraja, A review on the production of metal matrix MMCs through stir casting–Furnace design, properties, challenges, and research opportunities, J. Manuf. Process. 42 (2019) 213–245.
[10] S.E. Shin, D.H. Bae, Deformation behavior of aluminum alloy matrix MMCs reinforced with few-layer graphene, MMCs Part A, Applied Science and Manufacturing 78 (2015) 42–47.
[11] P.A. Rometsch, Y. Zhang, S. Knight, Heat treatment of 7xxx series aluminium alloys—some recent developments, Trans. Nonferrous Metals Soc. China 24 (7) (2014) 2003–2017.
[12] T. El-Bitar, F. Nouh, Omayma A. El-Kady, Hossam M. Yehia, Impact of graphene and hot-rolling on the microstructure and mechanical properties of aluminum matrix nano-composite. Research square, doi.org/10.21203/rs.3.rs-1258597/v1.
[13] B.T. Ramesh, Vinayak Koppad, T. Hemanth Raju, Fabrication of stir casting setup for metal matrix composite, IJSRD 5 (Issue 06) (2017).
[14] Wanwu Ding, Taili Chen, Xiaoyan Zhao, Yan Cheng, Xiaoxiong Liu, Lumin Gou, Investigation of microstructure of Al-5Ti-0.62C system and synthesis mechanism of TiC, Materials 13 (2020) 310, https://doi.org/10.3390/ma13020310.
[15] Shuwei Duan, Zhongli Liu, Fuqiang Guo, Yuzhe Pan, Precipitates evolution during artificial aging and their influence on mechanical properties of a cast Al-Cu-Li alloy, J. Mater. Res. Technol. 22 (2023), 2502-2 5 1 7.
[16] Niraj Nayan, K. Govind, Suseelan Nair, M.C. Mittal, K.N. Sudhakaran, Studies on Al–Cu–Li–Mg–Ag–Zr alloy processed through vacuum induction melting (VIM) technique, Mater. Sci. Eng. 454–455 (2007) 500–507.
[17] Na Jiang, G.A.O. Xiang, Z.H.E.N.G. Zi-qiao, Microstructure evolution of aluminum-lithium alloy 2195 undergoing commercial production, Transections of nonferrous metals society of china 20 (2010) 740–745.
[18] L. Wang, J. Jin, J. Cao, P. Yang, Q. Peng, Interaction of edge dislocations with graphene nanosheets in graphene/Fe composites, Crystals 8 (2018) 160, https://doi.org/10.3390/cryst8040160.
[19] J. Zhu, X. Liu, X. Zhou, Q. Yang, Strengthening effect of graphene-edge dislocation interaction in graphene reinforced copper matrix composites, Comput. Mater. Sci. 188 (2021) 110179.
[20] C. Polayya, C.S.P. Rao, G.B. Veeresh Kumar, et al., Synthesis and mechanical properties of graphene nanoparticles reinforced with aluminium alloy matrix composites, Nanotechnol. Environ. Eng. 8 (2023) 469–480, https://doi.org/10.1007/s41204-022-00305-6.
[21] H. Pan, Y. He, X. Zhang, Interactions between dislocations and boundaries during deformation, Materials 14 (2021) 1012, https://doi.org/10.3390/ma14041012.
[22] P. Ashwath, M. Venkatraman, Alicia Patel, M. Anthony Xavior, Andre Batako, Innovation in sustainable composite research: investigating graphene-reinforced MMCs for liquid hydrogen storage tanks in aerospace and space exploration, J. Mater. Res. Technol. 33 (2024), https://doi.org/10.1016/j.jmrt.2024.10.070. ISSN 2238-7854.
[23] Ashwath Pazhani, M. Venkatraman, M. Anthony Xavior, Synthesis and characterisation of graphene-reinforced AA 2014 MMC using squeeze casting method for lightweight aerospace structural applications, Mater. Des. 230 (2023) 111990.
[24] P. Lequeu, K.P. Smith, A. Daniélou, Aluminum-copper-lithium alloy 2050 developed for medium to thick plate, J. Mater. Eng. Perform. 19 (6) (2009) 841–847, https://doi.org/10.1007/s11665-009-9554-z.
[25] I. Häusler, R.D. Kamachali, W. Hetaba, B. Skrotzki, Thickening of T1 precipitates during aging of a high purity Al–4Cu–1Li–0.25Mn alloy, Materials 12 (2019) 30, https://doi.org/10.3390/ma12010030.
[26] M. Khushaim, T. Boll, J. Seibert, F. Haider, T. Al-Kassab, Characterization of precipitation in Al-Li alloy AA2195 by means of atom probe tomography and transmission electron microscopy, Adv. Condens. Matter Phys. 2015 (2015) 1–11, https://doi.org/10.1155/2015/647468.
[27] Xuanxi Xu, Guohua Wu, Liang Zhang, Xin Tong, Fangzhou Qi, Youjie Guo, Liangbin Li, Xunman Xiong, Cunlong Wang, Regulation of precipitation behavior among T1, S', and θ' phases in Al–Cu–Li-(Mg–Ag) alloys by optimizing Ag/Mg ratios, Mater. Sci. Eng., A 876 (2023) 145158, https://doi.org/10.1016/j.msea.2023.145158. ISSN 0921-5093.
[28] Xiaoxue Chen, Huakun Xi XinwuMa, Guoqun Zhao, Yongxiao Wang, Xiao Xu, Effects of heat treatment on the microstructure and mechanical properties of extruded 2196 Al-Cu-Li alloy, Mater. Des. 192 (2020) 108746.
[29] A. Fadavi Boostani, S. Yazdani, R. Taherzadeh Mousavian, S. Tahamtan, R. Azari Khosroshahi, D. Wei, Z.Y. Jiang, Strengthening mechanisms of graphene sheets in aluminium matrix nanocomposites, Mater. Des. 88 (2015) 983–989, https://doi.org/10.1016/j.matdes.2015.09.063.
[30] S.J. Andersen, C.D. Marioara, J. Friis, S. Wenner, R. Holmestad, Precipitates in aluminium alloys, Adv. Phys. X 3 (1) (2018), https://doi.org/10.1080/23746149.2018.1479984.

[31] Y. Jiang, Z. Tan, G. Fan, Z. Zhang, D.-B. Xiong, Q. Guo, D. Zhang, Nucleation and growth mechanisms of interfacial carbide in graphene nanosheet/Al composites, Carbon (2020), https://doi.org/10.1016/j.carbon.2020.01.032.
[32] I. Häusler, C. Schwarze, M.U. Bilal, D.V. Ramirez, W. Hetaba, R.D. Kamachali, B. Skrotzki, Precipitation of T1 and θ′ phase in Al-4Cu-1Li-0.25Mn during age hardening: microstructural investigation and phase-field simulation, Materials 10 (2017) 117, https://doi.org/10.3390/ma10020117.
[33] Z. Gao, J.H. Chen, S.Y. Duan, et al., Complex precipitation sequences of Al-Cu-Li-(Mg) alloys characterized in relation to thermal ageing processes, Acta Metall. Sin. 29 (2016) 94–103, https://doi.org/10.1007/s40195-016-0366-5.
[34] B. Decreus, A. Deschamps, F. De Geuser, P. Donnadieu, C. Sigli, M. Weyland, The influence of Cu/Li ratio on precipitation in Al–Cu–Li–x alloys, Acta Mater. 61 (6) (2013) 2207–2218, https://doi.org/10.1016/j.actamat.2012.12.041.
[35] W.S. AbuShanab, E.B. Moustafa, E. Ghandourah, M.A. Taha, Effect of graphene nanoparticles on the physical and mechanical properties of the Al2024-Graphene nanocomposites fabricated by powder metallurgy, Results Phys. 103343 (2020), https://doi.org/10.1016/j.rinp.2020.103343.
[36] D.G. Papageorgiou, I.A. Kinloch, R.J. Young, Mechanical properties of graphene and graphene-based nanocomposites, Prog. Mater. Sci. 90 (2017) 75–127, https://doi.org/10.1016/j.pmatsci.2017.07.004.
[37] J. Jayaseelan, A. Pazhani, A.X. Michael, J. Paulchamy, A. Batako, P.K. Hosamane Guruswamy, Characterization studies on graphene-aluminium nano composites for aerospace launch vehicle external fuel tank structural application, Materials 15 (2022) 5907, https://doi.org/10.3390/ma15175907.
[38] F. Ruffino, F. Giannazzo, A review on metal nanoparticles nucleation and growth on/in graphene, Crystals 7 (2017) 219, https://doi.org/10.3390/cryst7070219.
[39] J.A. Muñoz, R.E. Bolmaro, A.M. Jorge, et al., Prediction of generation of high- and low-angle grain boundaries (HAGB and LAGB) during severe plastic deformation, Metall. Mater. Trans. A 51 (2020) 4674–4684, https://doi.org/10.1007/s11661-020-05873-3.
[40] P. Gravier, F. Mas, A. Barthelemy, E. Boller, L. Salvo, et al., Pore closure in thick aluminum plate: from industrial hot rolling to individual pore observation, J. Mater. Process. Technol. 303 (2022) 117509, https://doi.org/10.1016/j.jmatprotec.2022.117509.
[41] J.R. Miller, P.M. Weaver, Temperature profiles in composite plates subject to time-dependent complex boundary conditions, Compos. Struct. 59 (2) (2003) 267–278, https://doi.org/10.1016/s0263-8223(02)00054-5.
[42] D. Chen, J. Li, K. Sun, et al., Graphene-reinforced metal matrix composites: fabrication, properties, and challenges, Int. J. Adv. Manuf. Technol. 125 (2023) 2925–2965, https://doi.org/10.1007/s00170-023-10886-4.
[43] A.D. Herron, S.P. Coleman, K.Q. Dang, D.E. Spearot, E.R. Homer, Simulation of kinematic Kikuchi diffraction patterns from atomistic structures, MethodsX (2018), https://doi.org/10.1016/j.mex.2018.09.001.
[44] G. Nolze, A. Winkelmann, Crystallometric and projective properties of Kikuchi diffraction patterns, J. Appl. Crystallogr. 50 (1) (2017) 102–119, https://doi.org/10.1107/s1600576716017477.
[45] A. Winkelmann, G. Nolze, G. Cios, T. Tokarski, Mapping of local lattice parameter ratios by projective Kikuchi pattern matching, Phys. Rev. Mater. 2 (2018) 123803, https://doi.org/10.1103/PhysRevMaterials.2.123803.
[46] M. Rühle, M. Wilkens, in: Robert W. Cahn, Peter Haasen (Eds.), Chapter 11 - Transmission Electron Microscopy, fourth ed.Physical Metallurgy, North-Holland, 1996, pp. 1033–1113, https://doi.org/10.1016/B978-044489875-3/50016-8. ISBN 9780444898753.
[47] Pulkit Garg, Pallav Gupta, Devendra Kumar, Om Parkash, Structural and mechanical properties of graphene reinforced aluminum matrix composites, J. Mater. Environ. Sci. 7 (5) (2016) 1461–1473. ISSN: 2028-2508.
[48] P. Liang, J. Zhang, N. Kong, H. Li, H. Zhu, The microstructure characteristics evolution of bulk high-purity silver for high relief application, Metals 13 (2023) 463, https://doi.org/10.3390/met13030463.
[49] H. Gassour, G.E.D.A.A. El-Magd, A. Mazen, et al., Characterization of aluminum composite reinforced by silver nanoparticles, Sci. Rep. 13 (2023) 17952, https://doi.org/10.1038/s41598-023-45059-6.
[50] Jenő Gubicza, Nguyen Q. Chinh, János L. Lábár, Géza Tichy, Zoltán Hegedűs, Cheng Xu, Terence G. Langdon, Stability of microstructure in silver processed by severe plastic deformation, Int. J. Mater. Res. 100 (6) (2009) 884–887, https://doi.org/10.3139/146.110113.
[51] H. Granbohm, J. Larismaa, S. Ali, L.-S. Johansson, S.-P. Hannula, Control of the size of silver nanoparticles and release of silver in heat treated SiO2-Ag composite powders, Materials 11 (2018) 80, https://doi.org/10.3390/ma11010080.
[52] D. Gray, Adam nykoruk McCaughan and Bhaskar Mookerji, Crystal Structure of Graphite, Graphene and Silicon (2009). https://api.semanticscholar.org/CorpusID:14384870.
[53] S.P. Coleman, M.M. Sichani, D.E. Spearot, A computational algorithm to produce virtual X-ray and electron diffraction patterns from atomistic simulations, J. Occup. Med. 66 (2014) 408–416, https://doi.org/10.1007/s11837-013-0829-3.
[54] G. Kimminau, B. Nagler, A. Higginbotham, W.J. Murphy, N. Park, J. Hawreliak, J.S. Wark, Simulating picosecond x-ray diffraction from shocked crystals using post-processing molecular dynamics calculations, J. Phys. Condens. Matter 20 (50) (2008) 505203, https://doi.org/10.1088/0953-8984/20/50/505203.